NOVEL MIXED LIGAND COPPER(I) COMPLEX AS EMITTER ENABLES HIGH-PERFORMANCE OLEDS WITH VERY LOW EFFICIENCY ROLL-OFF

N. Keerthi[1]*, K. Nagashri[2]

Abstract

The present study was concentrated on the synthesis of four coordinate mixed ligand copper(I) complexes containing 1,10-phenanthroline derivatives, which were produced from 1,10-phenanthroline-5,6-dione, substituted 1,2-aminobenzene and 1-(1-methyl-1H-pyrazol-4-yl) butane-1,3-di (acacp). The [CuL^{1-5}(acacp)] produced complexes were evaluated using FT-IR, UV-Vis, Raman, mass, molar conductance, and elemental analyses. The 1,10-Phenanthroline derivative coordinates to the copper(I) ion in a bidentate fashion via the N(imine) atoms which along with 3-hydroxy-1-(1-methyl-1H-pyrazol-4-yl)but-2-en-1-one form a tetracoordinate complex. The complex has a distorted square planar coordination environment. Complexes with non-electrolyte composition are visible in the molar conductance measurements. The metal complexes mentioned above can be prepared for OLED devices using the solution approach since they are soluble in organic solvents. Based on emissive compounds as the dopants, effective solution-processed green, yellow, and red emitting OLEDs are created. The mixed ligand copper complexes achieved a high external quantum efficiency (EQE) of 26.8% with an extremely low efficiency roll-off of 10% at the high luminance of 10 000 nits, but also provides 18 times longer operational lifetime than that of the non-sensitized reference device. This finding firstly demonstrates the use of Cu(I) complex as an efficient TADF sensitizer and paves the way for practical applications of TADF sensitized OLEDs. The observed results suggested that the Cu(I) complex with a 1,10-Phenanthroline backbone coated on the OLED device achieved good performances due to the copper complex as emitter contain an imidazole moiety at the backbone of the diimine ligand and other heterocyclic cores, which increases the aromatic π-system compared to other ligand systems.

Keywords: Metal complexes, OLED Emission, diodes, Efficiency, 1,10-Phenanthroline.

[1]*Research Scholar, Department of Chemistry, Manonmaniam Sundaranar University, Tirunelveli-627012, Tamil Nadu, India
[2]Department of Chemistry, Manonmaniam Sundaranar University, Tirunelveli-627012, Tamil Nadu, India.
Email: shrik1810@gmail.com

***Corresponding Author: -** N. Keerthi
*Research Scholar, Department of Chemistry, Manonmaniam Sundaranar University, Tirunelveli-627012, Tamil Nadu, India

DOI: 10.53555/ecb/2021.10.4.07

1. Introduction

The consumption of electric energy has been increasing due to the increase in world population and the consequent higher demand for modern electronic and lighting devices. This way, awareness has been raised to the need of alternative ways to reduce energy consumption by developing more efficient light emitting alternatives. For example, the luminous efficiency for conventional light bulbs is 16 lm/W and for fluorescent lamps it is 70 lm/W, whereas lamps based on light-emitting diodes (LEDs) can reach up to 300 lm/W [1]. Therefore, LED devices have been progressively replacing old lighting technologies. A state of the art LED is usually based on inorganic III-nitride semiconductors such as GaN and GaAs in which light is generated from a central point [2]. Organic light-emitting diodes (OLEDs) are also efficient emitting systems, however in their case light is generated planarly [3-8] from an emissive layer composed essentially by an organic material (undoped or doped).

During the past three decades, the emitters of the OLEDs have updated from the conventional fluorescence [9] to the phosphorescence [10] and to thermally activated delayed fluorescence [11] (TADF) materials with the aim of harvesting the 75% triplet excitons. Since heavy metal based phosphorescent emitters have high cost and environmental-unfriendly nature, TADF emitters have recently been regarded as the most promising emitters for OLEDs. Adopting TADF materials as emitters is the most popular method of constructing high-efficiency OLEDs [12, 13] Besides, another way to harvest triplet excitons is to introduce TADF materials as sensitizers for guest emitters in OLEDs [14–16]. In this strategy, a TADF sensitizer can harvest triplet exctions and up-convert them to singlet states (S1) through the reverse intersystem crossing (RISC) process. And then the S1 of the sensitizer can be transferred to the S1 of a guest emitter via non-radiative Förster resonance energy transfer (FRET) to realize theoretically 100% exciton utilization efficiency [17]. Finally, the singlet excitons on the guest emitter emit with high efficiencies. Based on this TADF sensitizing approach, very high external quantum efficiencies (EQEs) of over 30% have been obtained for TADF OLEDs in full-color regions [18, 19] In addition, utilizing the phosphorescent dopants as sensitizers is another way to make full use of excitons,[20] since a FRET from the triplet state (T1) of the phosphorescent sensitizer to the S1 of fluorescent guest can be demonstrated. Significant breakthroughs have also been achieved by Ir(III) phosphor- and Pt(II) phosphor-sensitized OLEDs [21, 22].

In this work, we present an overview of the development of OLED devices, in particular those based on Cu(I) complexes, which show potential to be one of the most efficient alternatives for energy saving in lighting. The focus of the current investigation was on the synthesis of four coordinate mixed ligand copper(I) complexes. The optical characteristics of the complexes depend on copper stability in the +1 oxidation state. Mass, molar conductance, FT-IR, UV-Vis, Raman, and elemental analyses were used to characterise the produced complexes. The 3-hydroxy-1-(1-methyl-1H-pyrazol-4-yl)but-2-en-1-one and 3-hydroxy-1-(1-methyl-1H-pyrazol-4-yl)butanone create a tetracoordinate complex, which is how the 1,10-phenanthroline derivative coordinates to the copper(I) ion in a bidentate manner. Tetrahedral coordination environment is disrupted in the complex. In order to identify structure-property interactions that are helpful for the manufacturing of OLED devices, structural and spectroscopic properties of the produced Cu(I) complexes were next subjected to elucidation.

2. Experimental

We bought all of our chemicals and solvents from Merck. By combining benzaldehyde, 1,10-phenanthroline-5,6-dione, and substituted-heterocyclic amines in acetic acid/NH_4Cl as the selected ligand, a variety of 1,10-phenanthroline derivatives with imidazole and pyrazole moieties were created utilising a "one-pot" technique. By combining copper acetate, ligands, and 1-(1-methyl-1H-pyrazol-4-yl) butane-1,3-dione and refluxing the mixture for six hours, we created several Cu(I) complexes (Scheme 1). By using column chromatography to purify them, all Copper(I) complexes were then examined by FAB-MS, 1H and 13C NMR, FT IR, Raman, cyclic voltammetry, molar conductance, and elemental analysis. A Shimadzu UV-VIS spectrophotometer was used to record UV-VIS spectra. On a Shimadzu FT-IR Affinity-1 spectrophotometer, IR spectra were captured. A Carl Earo elemental analyzer was used to conduct elemental analyses (CHN). Nicolet Fourier-transform spectrometer measurements of the Raman spectra were made. The conductivities were measured using a systronics conductivity meter.

Preparation of 1,10-Phenanthroline derivative:

1,10-phenanthroline (2 gm) was mixed with KBr (1.0 gm) and added to a three neck round bottom flask. Next, 20 mL of concentrated H_2SO_4 and 20 mL of concentrated HNO_3 were slowly added, drop by drop, to this solution. The mixture was heated for five hours. The hot yellow solution was slowly poured over 500 mL of ice and water to obtain a pH (adjusted to neutral with the addition of NaOH). The yellow collour product, 1,10-phenanthroline-5,6-dione, was further purified by crystallisation from 100% ethanol after solvent removal and extraction with $CHCl_3$.

1,10-phenanthroline-5,6-dione (20 mmol), 3-nitrobenzaldehyde (20 mmol), furan-2-amine/ thiazole-2-amine/pyrrole-2-amine (20 mmol), ammonium acetate (20 mmol), and glacial acetic acid (20 mL) were added to a hot solution mixture and heated at 100 °C for 20 minutes under reflux for six hours. Following the addition of 20 mL of water, the pH level was changed to 7.0 at room temperature. The mixture was filtered, vacuum-dried to produce a coloured precipitate, collected, and cleaned with water and trace amounts of ethanol. Filtration on a silicagel column was used to clean the crude product that had been dissolved in ethanol (60–100 mesh). In Scheme 1, the synthetic approach to produce the desired chemical was described.

Ligand (L^1): Mol. Formula: $C_{18}H_{10}N_4O$, Molecular weight: 298. Yield: 71%; CHN analysis: Theoretical; Nitrogen 18.78, Carbon 72.47, Hydrogen 3.38; Found: Nitrogen 18.73, Carbon 72.30, Hydrogen 3.29. UV (nm): 348, 254 nm. FT-IR (cm^{-1}): 3281υ (Ar O-H), 3083-3070 υ(Aromatic–H); 2959, 2887 υ(C–H); 1648 υ(C=N), 1220υ (Ar C-OH). ^{1}H-NMR (ppm): 10.7 (-OH, 1H, s) 6.7-7.9 (9H, m). ^{13}C-NMR (ppm) (DMSO-d^6) =152.5 (C=N of 1,10-Phen), 150.2 (C=N of pyrazine), 141.2 (C-N), 156.2 (C-OH). FAB MS: m/z 299. Ligand (L^2): Mol. Formula: $C_{19}H_{12}N_4$, Molecular weight: 296. Yield: 68%; CHN analysis: Theoretical ; Nitrogen 18.91, Carbon 77.01, Hydrogen 4.08; Found: Nitrogen 18.86, Carbon 76.93, Hydrogen 3.99. UV (nm): 344, 257 nm. FT-IR (cm^{-1}): 3080-3078 υ (Aromatic–H); 2954, 2889 υ(C–H); 1651 υ (C=N),. ^{1}H-NMR (ppm): 3.23 (-CH3, 3H, s) 6.9-7.7 (9H, m). ^{13}C-NMR (ppm) (DMSO-d^6) =152.3 (C=N of 1,10-Phen), 150.1 (C=N of pyrazine), 141.3 (C-N), 138.5 (C-CH_3). FAB MS : m/z 297. Ligand (L^3): Mol. Formula: $C_{18}H_{10}N_4$, Molecular weight: 282. Yield: 70%; CHN analysis: Theoretical; Nitrogen 19.85, Carbon 76.58, Hydrogen 3.57; Found: Nitrogen 19.80, Carbon 76.53, Hydrogen 3.49. UV (nm): 343, 254 nm. FT-IR (cm^{-1}): 3088-3076 υ(Aromatic–H); 2950, 2883 υ(C–H); 1642 υ(C=N),. ^{1}H-NMR (ppm): 6.7-7.9 (10H, m). ^{13}C-NMR (ppm) (DMSO-d^6): 152 (C=N of 1,10-Phen), 150.3 (C=N of pyrazine), 141.3 (C-N). FAB MS found m/z 283. Ligand (L^4): Mol. Formula: $C_{18}H_9N_5O_2$, Molecular weight: 337. Yield: 72%; CHN analysis: Theoretical; Nitrogen 20.76, Carbon 64. 08, Hydrogen 5.68, Oxygen 9.49; Found: Nitrogen 20.71, Carbon 63.97, Hydrogen 5.63, Oxygen 9.44. UV (nm) : 338, 254 nm. FT-IR (cm^{-1}): 3084-3073 υ(Aromatic–H); 2982, 2891υ(C–H); 1645 υ(C=N),. ^{1}H-NMR (ppm): 6.9-7.7 (9H, m). ^{13}C-NMR (ppm) (DMSO-d^6) = 152.6 (C=N of 1,10-Phen), 151.2 (C=N of pyrazine), 140.8 (C-NO_2). FAB MS: m/z 338. Ligand (L^5): Mol. Formula: $C_{18}H_9N_4Cl$, Molecular weight: 316. Yield: 76%; CHN analysis: Theoretical; Nitrogen 17.69, Carbon 68.25, Hydrogen 2.86; Found: Nitrogen 17.64, Carbon 68.17, Hydrogen 2.82. UV (nm) : 343, 247 nm. FT-IR (cm^{-1}): 3089-3071 υ(Aromatic–H); 2972, 2894υ(C–H); 1649 υ(C=N), 754 (C-Cl). ^{1}H-NMR (ppm): 6.7-7.8 (9H, m). ^{13}C-NMR (ppm) (DMSO-d^6) 152.2 (C=N of 1,10-Phen), 151.5 (C=N of pyrazine), 138.6 (C-Cl). FAB MS: m/z 317.

Preparation of copper chelates

The hot reacting solution of above mentioned ligand was added with 1-(1-methyl-1H-pyrazol-4-yl) and butane-1,3-dione (0.05 mol) in 50 mL and were mixed with copper acetate (0.05 mol) solution. Then, the reacting mixture was electrically stirred at RT and waited up to the precipitate formed. Then, the solid was separated and washed with methanol and hexane. The other metal complexes were prepared in the similar way.

Copper complex of L^1 : Mol. Formulae: $C_{28}H_{22}N_6O_5Cu$. Molecular wt. 586. Yield: 62%; CHN: Theoretical : Carbon 57.38, Hydrogen 3.78, Nitrogen 14.34, Copper 10.84; Found: Carbon 57.22, Hydrogen 3.60, Nitrogen 14.22, Copper 10.70. UV (nm): 334, 240 & 512 nm. FT-IR (KBr): 1172 (C–N), 1615 (C=N), 552 (Cu–N), 478 (Cu–O). FAB mass: 587 m/z[M+1]. Magnetic moment = 0 BM. Λm (Scm^2mol^{-1}) =80. Copper complex of L^2 : Mol. Formulae: $C_{29}H_{24}N_6O_4Cu$. Molecular wt. 584. Yield: 69%; CHN: Theoretical : Carbon 59.63, Hydrogen 4.14, Nitrogen 14.39, Copper 10.88; Found: Carbon 59.48, Hydrogen 4.05, Nitrogen 14.22, Copper 10.72. UV-Vis., (nm): 336, 254 & 506 nm. FT-IR (KBr): 1165 (C–N), 1640 (C=N), 554 (M–N), 482 (M–O). FAB mass: 585 m/z[M+1]. Magnetic moment = 0 BM. Λm (Scm^2mol^{-1}) =82.

Copper complex of L^3: Mol. Formulae: $C_{28}H_{22}N_6O_4Cu$. Molecular wt. 570. Yield: 63%; CHN: Theoretical : Carbon 58.99, Hydrogen 3.89, Nitrogen 14.74, Copper 11.15; Found: Carbon 58.65, Hydrogen 3.77, Nitrogen 14.60, Copper 11.04. UV-Vis., (nm): 344, 268 & 498 nm. FT-IR (KBr): 1174 (C–N), 1618 (C=N), 565 (M–N), 468 (M–O). FAB mass: 571 m/z[M+1]. Magnetic moment = 0 BM. Λm (Scm^2mol^{-1}) =95. Copper complex of L^4: Mol. Formulae: $C_{28}H_{21}N_7O_6Cu$. Molecular wt. 615. Yield: 67%; CHN: Theoretical : Carbon 54.68, Hydrogen 3.44, Nitrogen 15.94, Copper 10.33; Found: Carbon 54.52, Hydrogen 3.30, Nitrogen 15.82, Copper 10.21. UV-Vis., (nm): 330, 244 & 514 nm. FT-IR (KBr): 1177 (C–N), 1618 (C=N), 564 (Cu–N), 482 (Cu–O). FAB mass: 616 m/z[M+1]. Magnetic moment = 0 BM. Λm (S cm^2mol^{-1}) =86. Copper complex of L^5: Mol. Formulae: $C_{28}H_{21}N_6O_4ClCu$. Molecular wt. 604. Yield: 62%; CHN: Theoretical : Carbon 55.63, Hydrogen 3.50, Nitrogen 13.90, Copper 10.51; Found: Carbon 55.52, Hydrogen 3.38, Nitrogen 13.74, Copper 10.36. UV-Vis., (nm): 338, 260 & 508 nm. FT-IR (KBr): 1165(C–N), 1626 (C=N), 548 (Cu–N), 476 (Cu–O). FAB mass: 605 m/z[M+1]. Magnetic moment = 0 BM. Λm (S cm^2mol^{-1}) =76.

OLED fabrication and characterization.

Figure 1 depicts the architecture of OLED device manufacture with multiple layers of chemical molecules stacked and displayed. The solutions of PVK, PBD, and copper complex were dissolved in chlorobenzene before being combined into two solutions with concentrations of 10 weight percent and 20 weight percent, depending on the amount of solution ingested. In chlorobenzene, PEDOT was also dissolved. The Polyvinylcarbazole (PVK): 2([1, 1'biphenyl]4yl)5(4(tert-butyl) phenyl)1,3,4oxadaizole (PBD): copper complex—also known as a doping device—was used to make the EML. We bought PVK, PEDOT, and PBD from Sigma-Aldrich Co., Ltd. The devices were constructed on a square of indium tin oxide (ITO) glass that had been cleaned, had a 0.15 cm2 surface area, and had a sheet resistance of 10 /sq. The ITO glass square was subsequently spin-coated with PEDOT as a hole injection layer and the copper complex doped blend of PVK and PBD as the EML. For 10 minutes, the EML was allowed to anneal at 120°C. The EML was then coated with LiF as an electron injection layer and Al as a cathode using thermal evaporation at a high vacuum pressure of 2 104 Pa. A thickness/rate metre was used to measure the rate and thickness of the deposition. The exterior quantum efficiencies were calculated using a Si photodiode in an integrating sphere, and all of these procedures were carried out in a nitrogen-filled dry glove box with a photometer.

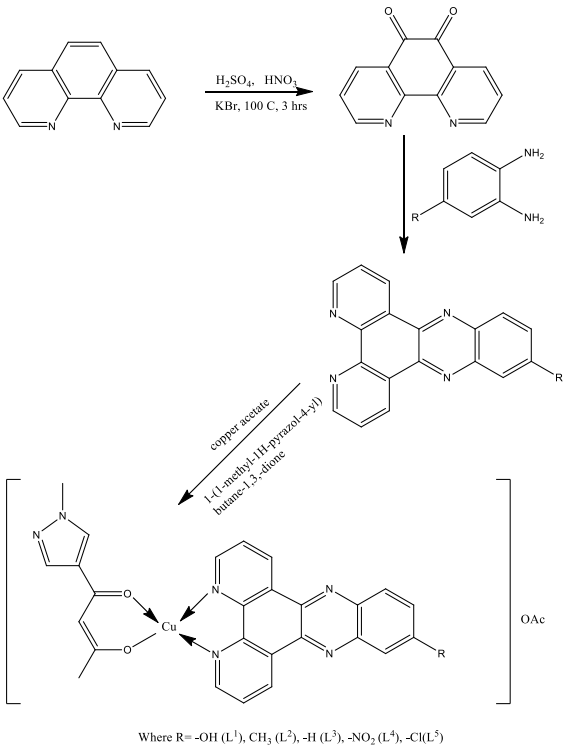

Scheme 1. Schematic representation of the synthesis of ligands and their copper complexes

3.Results and Discussion

Synthesis and Structural Characterization

Due to the prospect of creating extremely effective OLED devices with emission ranging from red to blue, at relatively cheap cost, Cu(I) complexes have gained attention during the past ten years. By gradually adding metal acetate solution to the ligand and pyrazole derivative in acetonitrile, copper-containing coordination compounds of ligands were produced. A copper (II) salt was converted into a highly stable copper (I) complex. Combining energy-dispersive X-ray spectroscopy, electrochemistry, UV/Vis spectroscopy, and X-ray photoelectron spectroscopy allowed researchers to analyse this chemical. Many attempts have been made to create crystals employing crystallisation with solvent mixes and low temperatures, but no success has been had. Regrettably, copper complex NMR and ESR experiments were ineffective (relaxation was very fast and the NMR signals are broad and weak intensity signal was observed). The structure of the compound was ascertained by combining various analytical and spectroscopic methods. Based on information from mass spectrometry elemental analysis, molar conductance, FTIR and electronic absorption spectroscopy, as well as ESR, the structures of the discovered complexes were determined. Electrochemical tests verified the copper's oxidation state in the complexes. The composition was further supported by evidence from elemental analyses. The ligand's donor characteristics are reduced by the heterocyclic structural core and electron-withdrawing substituent (NO_2) in the benzene ring's para position, which makes copper more stable in the oxidation state +1 than in the +2 and leads to the formation of complexes containing Cu^{1+}. The rigid and highly conjugated 1,10-Phenanthroline derivative also supports stability and photophysical properties. The complexes' proposed formula and the findings of the elemental analysis agreed well enough to support their purity. With the exception of displaying the effect of coordination to the metal, the IR spectra of the complexes display the distinctive bands of the respective free ligands. The hypothesised structures are congruent with the analytical and spectroscopic results. The complexes are insoluble in other organic solvents but soluble in acetonitrile and dimethyl sulfoxide. Based on elemental composition and an indicative 1:1 stoichiometric radio of the ligand and metal, the production of the ligand (L) and its metal chelates was determined. The electrolytic activity was determined to be 10-15 mho $mol^{-1}cm^2$ using molar conductivity measurements of metal chelate (0.001 M) in DMSO. According to the aforementioned experimental finding, the coordination complex is devoid of any counter anion [23]. The creation of a copper(I) complex is supported by the copper complex's partial solubility.

FT IR spectra

A comparison was made between the complex and free ligand's infrared spectral data. When complexed, these frequencies move to a lower wavenumber. The free phenanthroline ligand's bands are seen shifting in the spectra in the 1500–1250 cm^{-1} range. Particularly, the coordination of the "1,10-phen" nitrogen atoms to the metal ion is shown by a shifting of the peaks corresponding to the ring stretching frequencies vC=C and C=N at 1505 and 1421 cm^{-1} to higher frequencies at 1534 and 1450 cm^{-1} [21]. The vibrational spectra of copper complexes revealed two absorptions at 443 and 322 cm^{-1}, which can be attributed to vCu-N and Cu-O, respectively. The sharp band seen at 846 cm^{-1} in the free Schiff base ligand is caused by the phenazine ring (C-N-C) stretching frequency. This band doesn't shift much across all complexes, indicating that the thiophene sulphur was not involved in complex formation [24]. The stretching mode of the methyne group (CH) of the enolic form is responsible for the band at 3010 cm-1 in the infrared spectra of the acetylacetonato ligand. Four bands of stretching modes for the keto and enol forms exist in the region C=O and C=C. In contrast to the parent compound, the copper in the keto form of the vibration measured at 1729 cm-1 is coordinated to the carbonyl group. Yet a broad band at 1634 cm^{-1} is linked to the production of copper complexes and the keto-enol tautomerism, which is the enolic form of the carbonyl group. Two distinct peaks in the area of 1622–1418 cm^{-1} may be seen on the complicated spectrum. Assigned as C=O and C=C vibrations, respectively, are the bands at 1615(sh) and 1580 cm^{-1}. Because of this, the synthesised ligand molecules were coordinated with copper in a bidentate manner and with the auxillary ligand (a derivative of acetylacetone) in a bidentate fashion (through a carbonyl and an alcoholic group, respectively).

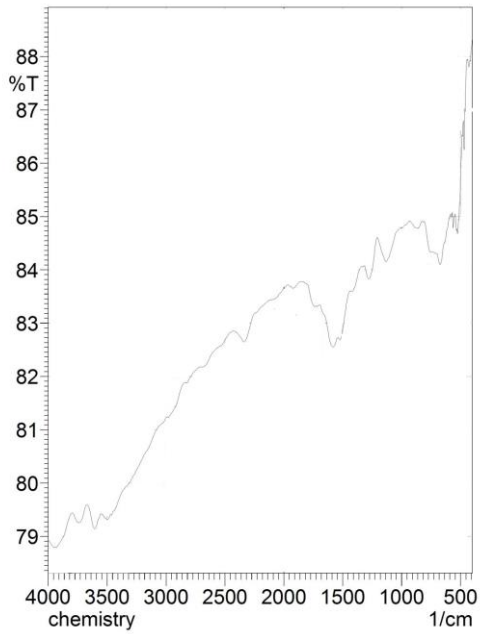

Figure 1. FT IR spectrum of ligand, L^1

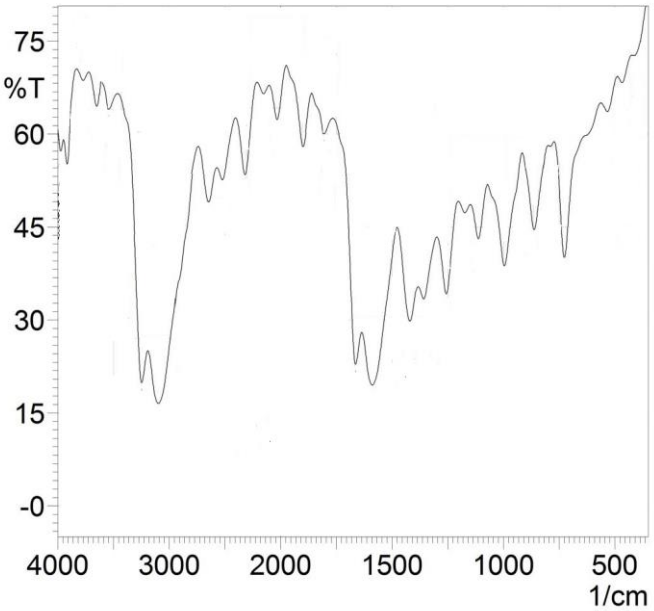

Figure 2. FT IR spectrum of mixed ligand copper of L^1

UV-Visible spectra

The experimental section contains the electronic spectral assignments for the free ligands and related complexes. The bands at 362 and 256 nm in the spectra of the free ligand (L^1) are attributable to the n→ π* transitions of the phenanthroline and furan moieties, respectively. Due to chelation or complexation, these absorption bands were displaced in the copper complex. The electronic transitions of n are pushed to a higher value due to the formation of the complexes with the copper when the wavelength of free ligands and the equivalent copper(I) complexes are compared. The Copper complex of L^1 exhibits weak and broad low-energy shoulders around 532 nm in addition to the high energy absorption bands, which is what gives the complex its yellow colour. Due to the low-energy transition between the electron-rich Cu(I) ion and the low-lying empty orbital in the N,N-chelate ligand, the similar trend was seen in the absorption spectra of other copper complexes. The Cu^{1+}-containing compounds are typically colourless. The inclusion of phenanthroline, phenazine core that signifies the colour of the copper complexes. The complexes' dark red hue appears to be caused by the UV region's strong ligand absorption band, which undergoes

bathochromic shift upon complexation with Cu^{1+}. Additionally, the band gap (Eg) of mixed ligand copper complexes of L^1–L^5 and acacp was calculated based on its UV/vis spectra in accordance with Kubelka–Munk theory,[12] and was discovered to be 2.90, 3.14, and 2.92 eV.

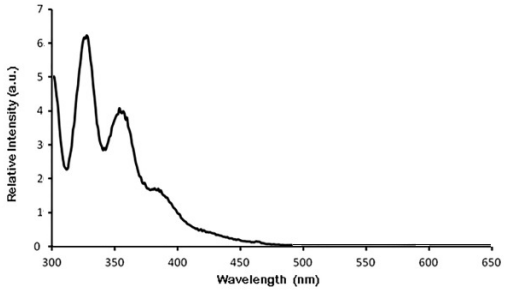

Figure 3. Electronic absorption spectrum of ligand

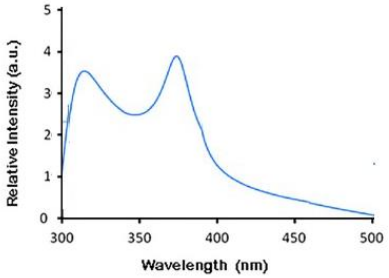

Figure 4. Electronic absorption spectrum of copper complex

Determination of the oxidation state of the copper

X-ray photoelectron spectroscopy was used to examine the copper's oxidation state (XPS). The binding energy peak was observed at 936.4 eV and no satellite peaks were visible in the copper complex of L^1's XPS spectra. This peak and lack of satellite peaks demonstrate that the copper is in the +1 oxidation state. All other complexes showed a similar pattern. The XPS was used to determine the functional groups.

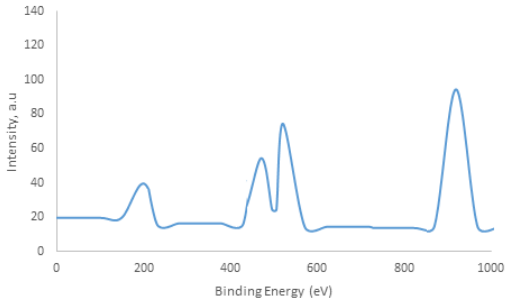

Figure 5. XPS spectrum of mixed ligand copper complex of L^1

In accordance with the research of Deng et al., the 1s electrons participating in a covalent connection between copper and nitrogen may have a binding energy of 416.5 eV at the peak in Figure 5. As one of the nitrogen atoms was possibly covalently bonded to copper, the [CuL1(acacp)] complex's above peak could indicate this. Two peaks with roughly identical intensities that correspond to the oxygen atom's 1s core level in the C=O and C-O functional groups, respectively, were found to fit the O 1s spectrum. These peaks' binding energies (BEs) were 534.0 and 536.5 eV. These peaks show a range of intensities, proving that these metal-coordinated oxygen-containing groups. Also, the peak at 290.6 eV denotes carbon atoms that are doubly bound to oxygen atoms (C=O), while the peak at 285.5 eV indicates the existence of carbon atoms that are singly bonded to oxygen atoms in the ligand (L^1).

ii) Electrochemical technique

Using cyclic voltammetry, the copper(II) acetate was used to prepare several copper complexes and determine the oxidation state of the mixed ligand copper complex as Cu^0, Cu^I, or Cu^{II}. Cyclic voltammetry was used to analyse the electrochemical behaviour of the copper complex in DMSO with 0.1 mol L^{-1} of tetrabutylammonium perchlorate as a supporting electrolyte (Fig.6). When compared to a saturated calomel electrode (SCE), the free ligand L^1 showed an irreversible process that might be attributed to the electrochemical oxidation of the ligand at a potential of roughly 0.80 V. The mixed-ligand copper complex of L^1 exhibited quasi-reversible oxidation-reduction properties; the oxidation potential and reduction potential were respectively at 0.10 and 0.26 V, which corresponds to the conversion of $Cu^{1+/2+}$.

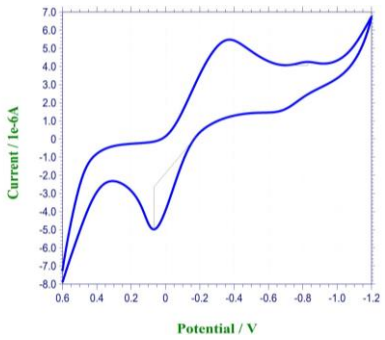

Figure 6. Cyclic voltammogram of mixed ligand copper complex of L^1

In the current study, thermal analysis was carried out to get valuable information about the thermal stability of the synthesized complexes and decide whether water molecules are outside or inside the inner coordination sphere of the metal. The TGA result (Figure 7) shows that the copper complex of L^1 can thermally decompose at a temperature of up to 322 °C, which satisfies the need for vacuum-thermal deposition (at about 260 °C). Thermogravimetric and differential thermal analysis (TGA and DTA) was used to investigate the thermal behaviour of this complex in an air atmosphere (Figure 5). According to the findings, this compound is stable up to about 310°C. The melting of the complex is shown by the endothermic peak in the DTA curve at 145°C. The removal of organic groups from the complex structure is what causes a significant weight loss and an extreme exothermic peak to appear in the TGA and DTA curves of produced complexes in the temperature range of 320 to 450°C. Copper oxide particles are related to the residual component over 500°C. When fabricating devices, the thermal robustness of these materials helps produce uniform, smooth amorphous films, which is one of the crucial requirements for achieving very stable device performance. The doped films' surfaces had homogenous surface morphologies and extremely low root-mean-square roughness values of 0.35, 0.56, and 0.46 nm, respectively. According to these findings, host materials have superior thermal and morphological stability, which helps to improve device stability and electroluminescence (EL) performance while the device is in operation.

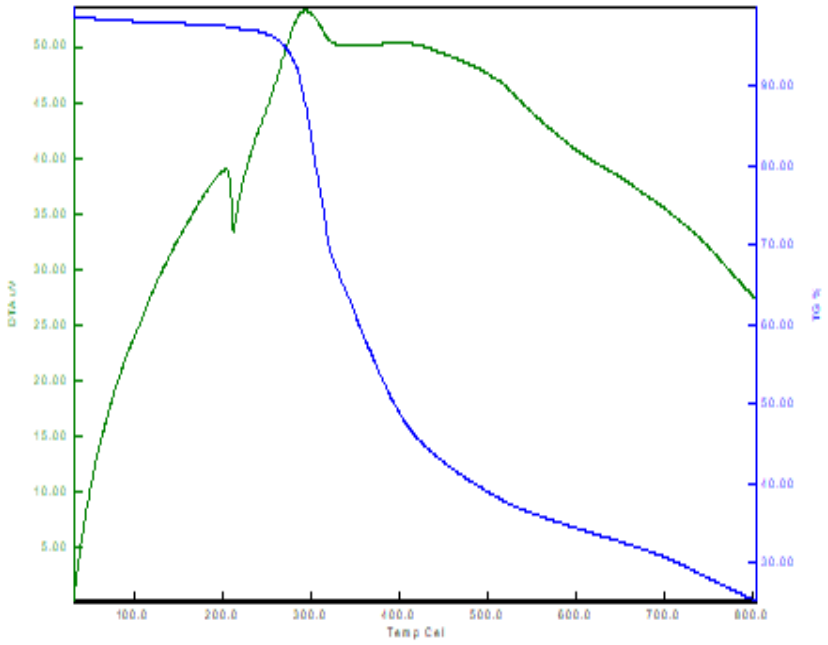

Figure 7. TGA profile of mixed ligand copper complex of L^1

Mass spectra

The molecular weight of the ligand and its metal chelates were verified by the FAB mass method. The observed molecular ion is identified as the stoichiometric [CuL^1(acacp)] chelate and supported by elemental proportions & molar conductance measurements. The mass spectrum of the ligand provides evidence in favour of the suggested formula (molecular ion m/z 299). The molecular mass peak of the copper complex, observed at 587, confirms the monomeric state of the metal chelate. Moreover, the mass spectra exhibit a variety of peaks that indicate the complexes' progressive disintegration through time with increasing intensity, providing evidence of fragment stability. As a result, the molecular stoichiometry [ML(acacp)] is verified by the molecular weight and conductivity values of complexes.

OLED Devices

The OLED device architecture with the Cu(I) complexes bearing the phenazine modified 1,10-Phenanthroline ligands were prepared and tested. With respect to the above, the auxillary materials were selected for the building of OLED layers resolutely, the energy of the HOMO and LUMO levels of the copper complexes were determined. The photo emission yield spectroscopy (PYS) method in combination with absorption spectroscopy was taken. The HOMO energy of the materials was determined by using the PYS method. Then the HOMO− LUMO energy gap (Eg) was calculated with the help of the absorption band and then the LUMO energy value was obtained using the inverse formula.

$$LUMO = HOMO - Eg$$

OLED device performance, all the prepared copper complexes were inserted into the device within the same heterostructure ITO (120−160 nm)/PEDOT:PSS (50 nm)/ poly TPD (15 nm)/20 wt % emitter:host (20 nm)/TPBi (30 nm)/LiF (1 nm)/Al (>100 nm) (with ITO = indium tin oxide, PEDOT:PSS = poly(3,4 ethylenedioxythiophene): poly (styrenesulfonate), poly TPD = poly(4 butyltriphenylamine and TPBi = 2,2′,2″ (1,3,5 benzinetriyl) tris(1 phenyl 1 H benzimidazol)). As host material, either CBP, CBP:TcTa or DMFL CBP (2,7 bis(carbazol 9 yl) 9,9 dimethylfluorene) were used. The starting point for the host material optimization was CBP. CBP is a well known high quality films of CBP could be deposited from solution. Zhang and co workers showed that CBP doped with TcTa in a 7:3 ratio led to a significant increase of the device efficiency. Poly TPD was chosen as hole transport layer because of its insolubility in most solvents after post treatment (annealing at 220 °C for 30 min in an argon glovebox).83 As electron transport layer (ETL) and hole transport layer (HTL) the well known and often used TPBi and PEDOT:PSS materials were selected.

The best host material was chosen by the comparison of the performance of a series of OLED devices based on Cu(I) complex emitter. The HOMO− LUMO levels of CBP:TcTa matched best with those of the copper emitter so that the holes and electrons recombine almost exclusively in the emitter molecules. In conclusion all copper emitter materials were tested in the heterostructure ITO (120−160 nm)/PEDOT:PSS (50 nm)/ poly TPD (15 nm)/20 wt % emitter:CBP:TcTa (7:3) (20 nm)/TPBi (30 nm)/LiF(1 nm)/Al (>100 nm), in which the emitter material was CuL^1 to CuL^5. To enable a proper comparison of the performance of the obtained OLED devices, the electroluminescence (EL) spectra were measured at the same conditions, only the integration time was varied when measuring the EL intensity. Thus, the intensity is given in sec^{-1}, which corresponds to the counts divided by the integration time.

The brightness of the devices based on the copper emitters having ligand L^4 reached 2450 Cd/m^2 and 2860 Cd/m^2 and the current efficiency up to 3.8 Cd/A and 2.6 Cd/A, respectively. For the devices based on the other Cu(I) complexes, brightnesses in the range of 380−2600 Cd/m^2 was found. The current efficiencies of these OLED devices were in the range of 0.76−5.35 Cd/A. In order to achieve a maximum brightness, the OLED devices based on the best performing materials (EML with CuL^5) were further optimized. The emission layer thickness was varied in order to decrease the turn on voltage and the charge carrier balance. The thickness of the EML was tuned by changing the spin coater frequency rate. A frequency of 1060 rpm gave a 45 nm layer (OLED-D1), 1500 rpm resulted in 30 nm (OLED-D2), and with up to 2120 rpm, a thinner EML of 15 nm (OLED-D3) was realized. The device with the thickest emission layer (OLED-D1) showed the lowest turn on voltage (4 V) and the highest brightness of up to 5900 Cd/m^2. In comparison to the photoluminescence of the Cu(I) complexes in doped films (20 wt % in CBP:TcTa (7:3)) at ambient temperature, the electroluminescence was slightly shifted. The electroluminescence originates from the Cu(I) complexes and not from the matrix, while for the photoluminescence, a

slight contribution from the matrix is visible. In general, the emission of the doped films and the corresponding OLEDs are comparable.

The efficiency of OLEDs is extremely sensitive to the perfect surface of materials, a further increase of the efficiency and brightness of the devices would have required other OLED manufacturing equipment up to professional level, which was unfortunately not accessible to us. This resulted in lower efficiencies of the obtained OLED devices relative to the previously published results for the Cu(I) complexes of the same nature. At the same time, the obtained brightness and efficiency are on the same level or above the values obtained for similar compounds in literature, which shows the advantages of the novel Cu(I) complexes in combination with the used stack architecture in the OLED device. All in all, the best OLED performance of this series of Cu(I) complexes with phosphino modified NP bridging ligands was demonstrated by OLED-D3 with the copper emitter CuL^5 bearing the triple methylated NP bridging ligand with a high brightness of 5900 Cd/m2 and a good current efficiency of 3.79 Cd/A.

To evaluate the effect of copper complexes as emitter in EL process, multilayer OLEDs were fabricated. The reference devices based on mCBP: 20 wt% PXZMePM: 1 wt% BN3 (device B2) and mCBP: 1 wt% BN3 (device C2) were also fabricated parallel. Figure 8 and 9 depicted the current density and luminance verse voltage curves. A device D3 exhibited the lowest turn-on voltage of 2.8 V, arising from the better charge carrier transport and injection ability of copper complex of L5. Figure 8 showed the EL spectra for the devices D1-D3. As expected, the device D3 based on copper complexes as emitter demonstrated a high maximum EQE of 26.5% with well-alleviated efficiency roll-off, which is the highest value for the MR-TADF OLEDs in the yellow emission region due to balanced charge carrier transport and injection ability as mentioned above, leading to the better performance in EL process. Even at the high luminance of 10 000 cd m^{-2}, the device D3 still remained a high EQE of 10.5%. The quick RISC process of copper complexes could help decrease the triplet exciton concentration and thereby relieve the quenching process in OLEDs caused by the aggregation of triplet excitons. This significant improvement of operational lifetime of the copper complexes as emitter OLED device proved the validity of our strategy of introducing Cu(I) complex as TADF sensitizer for MR-TADF emitters.

Table 1. Electroluminescence data of devices D1-D3 with copper complexes of L^1

Device	Voltage [V]	EQE max [%]	EQE@10 000 cd m^{-2}/ roll-off [%]	EQE@5 000 cd m^{-2}/roll-off [%]
D1	2.6	28.5	11.6/56.2	10.5/60.4
D2	3.5	20.8	7.9/56.4	6.7/63.0
D3	4.2	21.6	2.4/89.8	1.7/92.8

The turn-on voltage recorded at a luminance of 2 cd m^{-2}

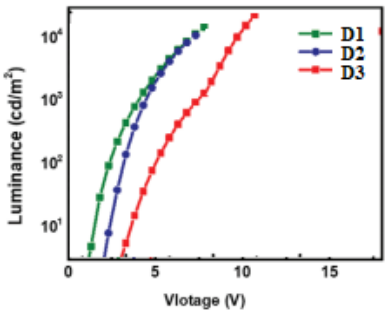

Figure 8. Brightness–voltage curves of devices D1-D3

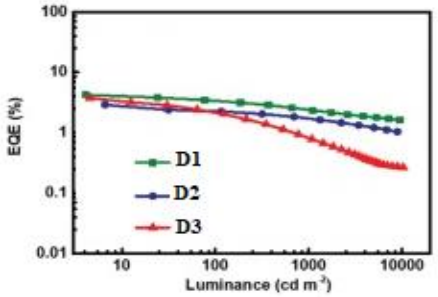

Figure 8. EQE versus luminance curves for devices D1-D3

Conclusion

In continuation of our previous research work, the 1,10-Phenanthroilne was modified with phenazine moiety instead of pyrrazole/ thiophene core with para substituted ligands was investigated in this work. The resulting phenazine modified 1,10-Phenanthroline ligand derived copper complexes were completely characterized and tested in solution processed organic light emitting diodes. The prepared copper complexes as an TADF sensitizer. The blue fluorescent OLED based on the copper complexes exhibited 5 times higher EQE than that of the non-sensitized reference device, but also exhibited 15 times longer operational lifetime. More importantly, the device based on copper complexes experienced slow efficiency roll-off behavior at high luminance: a record-high EQE of 12.8% at the ultrahigh luminance of 10 000 cd m^{-2}.

References

1. M. A. Baldo, D. F. O'Brien, Y. You, A. Shoustikov, S. Sibley, M. E. Thompson, S. R. Forrest, Nature 1998, 395, 151.
2. H. Uoyama, K. Goushi, K. Shizu, H. Nomura, C. Adachi, Nature 2012, 492, 234.
3. J.-X. Chen, K. Wang, Y.-F. Xiao, C. Cao, J.-H. Tan, H. Wang, X.-C. Fan, J. Yu, F.-X. Geng, X.-H. Zhang, C.-S. Lee, Adv. Funct. Mater. 2021, 31, 2101647.
4. P. Wei, D. Zhang, L. Duan, Adv. Funct. Mater. 2019, 30, 1907083.
5. C. W. Tang, S. A. VanSlyke, Appl. Phys. Lett. 1987, 51, 913.
6. Endo, M. Ogasawara, A. Takahashi, D. Yokoyama, Y. Kato, C. Adachi, Adv. Mater. 2009, 21, 4802.
7. X. Gong, P. Li, Y.-H. Huang, C.-Y. Wang, C.-H. Lu, W.-K. Lee, C. Zhong, Z. Chen, W. Ning, C.-C. Wu, S. Gong, C. Yang, Adv. Funct. Mater. 2020, 30, 1908839.
8. W. Zeng, T. Zhou, W. Ning, C. Zhong, J. He, S. Gong, G. Xie, C. Yang, Adv. Mater. 2019, 31, 1901404.
9. H. Nakanotani, T. Higuchi, T. Furukawa, K. Masui, K. Morimoto, M. Numata, H. Tanaka, Y. Sagara, T. Yasuda, C. Adachi, Nat. Commun. 2014, 5, 4016.
10. D. Zhang, L. Duan, C. Li, Y. Li, H. Li, D. Zhang, Y. Qiu, Adv. Mater. 2014, 26, 5050. [11] L.-S. Cui, A. J. Gillett, S.-F. Zhang, H. Ye, Y. Liu, X.-K. Chen, Z.-S. Lin, E. W. Evans, W. K. Myers, T. K. Ronson, H. Nakanotani, S. Reineke, J.-L. Bredas, C. Adachi, R. H. Friend, Nat. Photonics 2020, 14, 636.
11. D. Zhang, X. Song, A. J. Gillett, B. H. Drummond, S. T. E. Jones, G. Li, H. He, M. Cai, D. Credgington, L. Duan, Adv. Mater. 2020, 32, 1908355.
12. S. O. Jeon, K. H. Lee, J. S. Kim, S.-G. Ihn, Y. S. Chung, J. W. Kim, H. Lee, S. Kim, H. Choi, J. Y. Lee, Nat. Photonics 2021, 15, 208.
13. Yin, D. Zhang, Y. Zhang, Y. Lu, R. Wang, G. Li, L. Duan, CCS Chem. 2020, 2, 1268.
14. Y. Liu, X. Xiao, Y. Ran, Z. Bin, J. You, Chem. Sci. 2021, 12, 9408.
15. P. Heimel, A. Mondal, F. May, W. Kowalsky, C. Lennartz, D. Andrienko, R. Lovrincic, Nat. Commun. 2018, 9, 4990.
16. S. Nam, J. W. Kim, H. J. Bae, Y. M. Maruyama, D. Jeong, J. Kim, J. S. Kim, W.-J. Son, H. Jeong, J. Lee, S.-G. Ihn, H. Choi, Adv. Sci. 2021, 8, e2100586.
17. W. Zeng, H.-Y. Lai, W.-K. Lee, M. Jiao, Y.-J. Shiu, C. Zhong, S. Gong, T. Zhou, G. Xie, M. Sarma, K.-T. Wong, C.-C. Wu, C. Yang, Adv. Mater. 2018, 30, 1704961.
18. Y. Xiang, P. Li, S. Gong, Y.-H. Huang, C.-Y. Wang, C. Zhong, W. Zeng, Z. Chen, W.-K. Lee, X. Yin, C.-C. Wu, C. Yang, Sci. Adv. 2020, 6, eaba7855.
19. H. Wang, L. Meng, X. Shen, X. Wei, X. Zheng, X. Lv, Y. Yi, Y. Wang, P. Wang, Adv. Mater. 2015, 27, 4041.
20. W. J. Chung, J. Y. Lee, J. Mater. Chem. C 2021, 9, 7458.

21. N. Aizawa, A. Matsumoto, T. Yasuda, Sci. Adv. 2021, 7, eabe5769.
22. L. Yang, V. Kim, Y. Lian, B. Zhao, D. Di, Joule 2019, 3, 2381.
23. R. Hamze, J. L. Peltier, D. Sylvinson, M. Jung, J. Cardenas, R. Haiges, M. Soleilhavoup, R. Jazzar, P. I. Djurovich, G. Bertrand, M. E. Thompson, Science 2019, 363, 601.
24. A.Ying, Y.-H. Huang, C.-H. Lu, Z. Chen, W.-K. Lee, X. Zeng, T. Chen, X. Cao, C.-C. Wu, S. Gong, C. Yang, ACS Appl. Mater. Interfaces 2021, 13, 13478.
25. S. Romanov, L. Yang, S. T. E. Jones, D. Di, O. J. Morley, B. H. Drummond, A. P. M. Reponen, M. Linnolahti, D. Credgington, M. Bochmann, Chem. Mater. 2019, 31, 3613. [27] F. Chotard, V. Sivchik, M. Linnolahti, M. Bochmann, A. S. Romanov, Chem. Mater. 2020, 32, 6114.
26. P. J. Conaghan, C. S. B. Matthews, F. Chotard, S. T. E. Jones, N. C. Greenham, M. Bochmann, D. Credgington, A. S. Romanov, Nat. Commun. 2020, 11, 1758.
27. H. H. Cho, A. S. Romanov, M. Bochmann, N. C. Greenham, D. Credgington, Adv. Opt. Mater. 2020, 9, 2001965